

Supporting Information

Domain Architectures and Grain Boundaries in Chemical Vapor Deposited Highly Anisotropic ReS₂ Monolayer Films

Kedi Wu¹, Bin Chen¹, Sijie Yang¹, Gang Wang², Wilson Kong¹, Hui Cai¹, Toshihiro Aoki¹, Emmanuel Soignard¹, Xavier Marie², Aliya Yano¹, Aslihan Suslu¹, Bernhard Urbaszek², and Sefaattin Tongay^{1*}

¹School for Engineering of Matter, Transport and Energy, Arizona State University, Tempe, AZ 85287, USA

²Universit e de Toulouse, INSA-CNRS-UPS, LPCNO, 135 Av. Rangueil, 31077 Toulouse, France

Corresponding author email: Sefaattin.tongay@asu.edu

Section S1. Effect of temperature, flow-rate, and precursor amount on the ReS₂ vapor phase growth

The temperature dependent studies in the 490-520 °C range reveal that increasing the temperature decreases the nucleation density but yields larger sized flakes at atmospheric pressure (**Figure S1a-c**). This finding is consistent with previous studies in graphene¹ and MoS₂² monolayers. However, ReS₂ monolayers grown at higher (>520 °C) temperatures take more complex shapes with multi-layer growth, thus the ideal temperature for the high-quality formation of these triangular flakes appears to be in the range of 490-520 °C.

In our studies, we find that the growth temperature, initial loading amount of NH₄ReO₄ and overall flow-rate make large changes in overall coverage and domain structure of ReS₂ layers (**Figure S1d-f**). For example, increasing the NH₄ReO₄ precursor amount from 10 mg to 50 mg at 500 °C and 50 sccm flow-rate, results in much smaller domain sizes and higher nucleation densities (**Figure S1d-f**) due to much increased Re intermediate oxide concentration. This implies that NH₄ReO₄, i.e., rhenium sub-oxides, controls the nucleation density and large-area growth in agreement with similar findings for MoO₃ in MoS₂ growth. High flow rate of carrier gas may promote the mass transfer that contributes to the increase in the crystal growth rate. In this case atoms do not have enough time to move into the right lattice locations, where crystal domains could have the lowest surface free energy, and the probability of defect formation increases therefore under high flow rate conditions, the ReS₂ crystals are more likely to grow under kinetic conditions which is resulting in the formation of dendritic morphologies rather than the thermodynamic ones. Similarly, decreasing the flow-rate from 50 sccm to 10 sccm significantly increases the domain sizes and stabilizes hexagonal features possibly due to much wider diffusion boundary layer and limited precursor supplies in line with trends for NH₄ReO₄ precursor amount. Overall, it appears that hexagonal ReS₂ monolayers are synthesized at low temperature, NH₄ReO₄ precursor amount, and flow-rate conditions, whereas triangular features are observed at slightly higher temperatures.

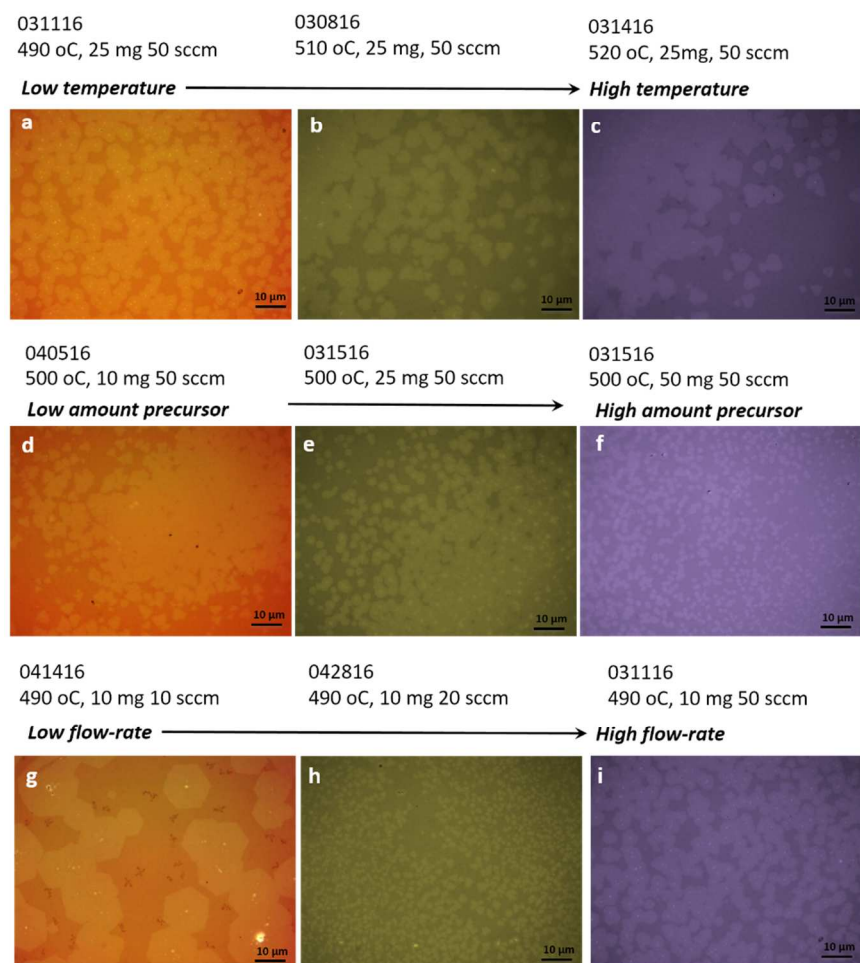


Figure S1 Optical images taken from ReS₂ monolayers deposited onto c-cut sapphire substrates at various conditions such as **a-c** low to high temperatures, **d-f** low to high precursor amount, and **g-i** low to high gas flow-rates.

Section S2 Angle resolved measurements on Bulk and few-layer ReS₂

Figure S2 shows polar plots for 153 cm⁻¹ and 214 cm⁻¹ peaks, the most two prominent Raman peak of ReS₂, for exfoliated ReS₂ thin (<5 nm) and thick (<50 nm) samples. As shown below, the polar plot of 214 cm⁻¹ peak aligns relatively well with the *b*-axis direction of the exfoliated ReS₂ crystal. On the contrary, the 153 cm⁻¹ peak does not line with any of the distinguishable features of exfoliated ReS₂. This phenomena is related to the fact that 214 cm⁻¹ peak involves atomic displacements of S and Re atoms along the *b*-axis whereas 153 cm⁻¹ peak does not have well defined atomic displacement along any high symmetry points (along *b*- or *a*-axis)³. This finding is fully consistent with prior findings and similar reports on ReS₂⁴⁻⁶, and allows us to define the *b*-axis direction from angle resolved Raman spectroscopy measurements. We, however, note that there is a slight offset (~10 degrees) from absolute *b*-axis direction. For this reason, angle resolved Raman measurements on 214 cm⁻¹ yields the crystalline orientation of *b*-axis when offset by 10 degrees. This effect was accounted in identifying the absolute *b*-axis direction from the maximum angle at which Raman intensity of 214 peak is maximized. This can be

seen in triangular and hexagonal flakes: Compare **Figure 2b** to **Figure 2d-e** and **Figure 2g** to **Figure 2h**. Similar offset was also mentioned in earlier studies^{4,5}.

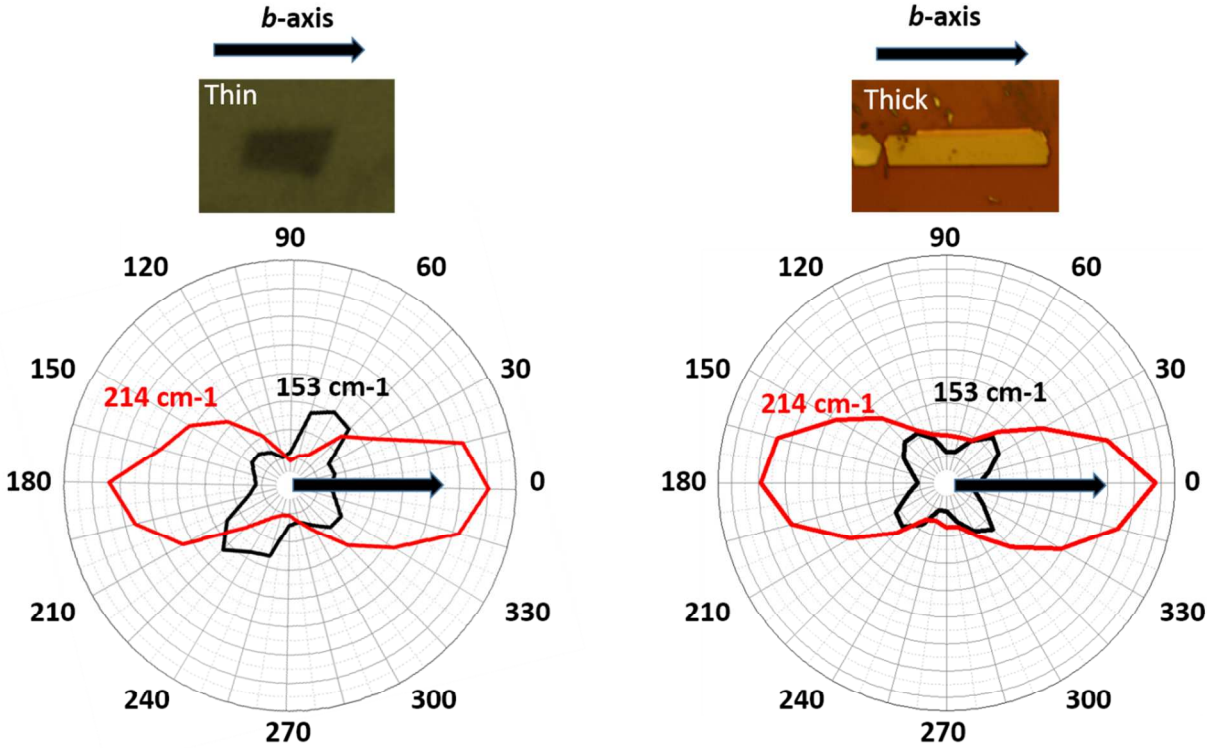


Figure S2. Angle-dependent Raman for Exfoliated thick (thickness > 50 nm) and thin (thickness < 5nm) ReS_2 samples.

Section S3 Angle-resolved reflectivity measurements on the hexagonal monolayer ReS_2

The reflectivity measurements are performed at 4K. A broadband white light (tungsten-halogen lamp) is focused on the hexagonal monolayer ReS_2 sample by a 50X objective with a spot size about $2 \mu\text{m}$, which is smaller than the triangle domain size. The excitation and detection are both linearly polarized along the same direction. An achromatic half wave plate is used to change the polarization angle with respect to the sample. The reflected signal from the sapphire substrate and the ReS_2 flake are dispersed by a spectrometer and detected with a Si-CCD as shown in the **Figure S3** black and red curves. The reflectivity is deduced by $(R_{\text{Sample+Sapphire}} - R_{\text{Sapphire}}) / R_{\text{Sapphire}}$ as plotted in Fig.S3 (blue curve), where $R_{\text{Sample+Sapphire}}$ and R_{Sapphire} represent the reflectance from ReS_2 on sapphire substrate, and the pure sapphire substrate respectively. Here in **Figure S3** the results with excitation and detection polarization angle at 30° are shown. The integrated intensity of reflectivity curves from 1.8 eV to 1.9 eV (shaded region in **Figure S3**) of all the angles are used to generate the data points in **Figure 2f** in main text, which depicts the anisotropy between different domains. The slight birefringence of the substrate alone has been measured separately and is subtracted from the ReS_2 reflectance data.

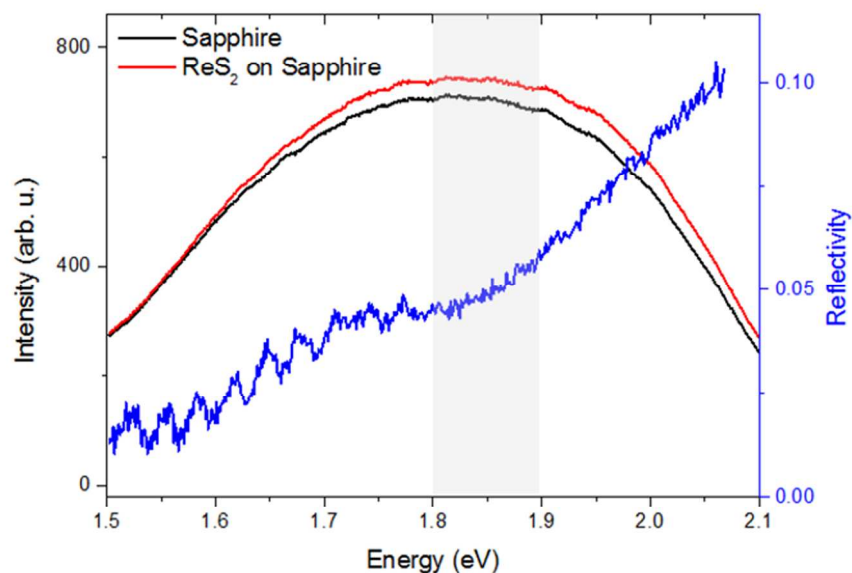


Figure S3 Reflectivity measurements at 30° performed at cryogenic (4K) temperatures on one sub-domain of hexagonal ReS_2 flake.

Section S4 Raman mapping at 214 cm^{-1} on a hexagonal flake grown under non-ideal conditions

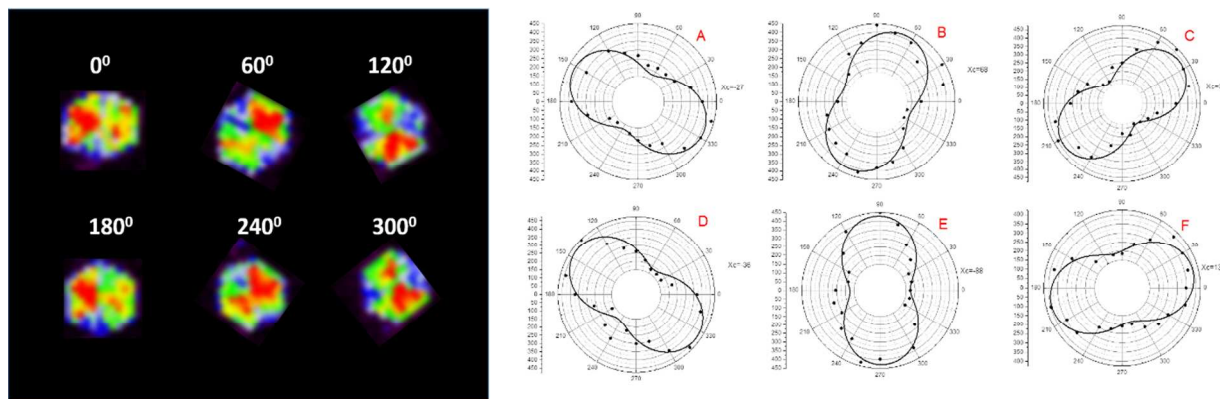


Figure S4. (left) Raman mapping at 214 cm^{-1} peak position and Angle-dependent Raman for various domains (from A to F).

Note: The authors declare no competing financial interest."

References

1. Vlassioug, I.; Smirnov, S.; Regmi, M.; Surwade, S. P.; Srivastava, N.; Feenstra, R.; Eres, G.; Parish, C.; Lavrik, N.; Datskos, P.; Dai, S.; Fulvio, P. *The Journal of Physical Chemistry C* **2013**, *117*, (37), 18919-18926.

2. Najmaei, S.; Liu, Z.; Zhou, W.; Zou, X.; Shi, G.; Lei, S.; Yakobson, B. I.; Idrobo, J.-C.; Ajayan, P. M.; Lou, J. *Nat Mater* **2013**, *12*, (8), 754-759.
3. Tongay, S.; Sahin, H.; Ko, C.; Luce, A.; Fan, W.; Liu, K.; Zhou, J.; Huang, Y. S.; Ho, C. H.; Yan, J.; Ogletree, D. F.; Aloni, S.; Ji, J.; Li, S.; Li, J.; Peeters, F. M.; Wu, J. *Nat Commun* **2014**, *5*, 3252.
4. Chenet, D. A.; Aslan, O. B.; Huang, P. Y.; Fan, C.; van der Zande, A. M.; Heinz, T. F.; Hone, J. C. *Nano Letters* **2015**, *15*, (9), 5667-5672.
5. Hart, L.; Dale, S.; Hoyer, S.; Webb, J. L.; Wolverson, D. *Nano Letters* **2016**, *16*, (2), 1381-1386.
6. He, R.; Yan, J.-A.; Yin, Z.; Ye, Z.; Ye, G.; Cheng, J.; Li, J.; Lui, C. H. *Nano Letters* **2016**, *16*, (2), 1404-1409.